AGU PUBLICATIONS

JGR

Journal of Geophysical Research: Space Physics

RESEARCH ARTICLE
10.1002/2017JA024039

Key Points:
- Statistical study of 400 periods of pulsating aurora has been conducted
- Auroral peak emission height decreases about 8 km at the start of a pulsating aurora event
- Majority of the events include pulsating aurora on both hemispheres

Correspondence to:
N. Partamies,
noora.partamies@unis.no

Citation:
Partamies, N., D. Whiter, A. Kadokura, K. Kauristie, H. Nesse Tyssøy, S. Massetti, P. Stauning, and T. Raita (2017), Occurrence and average behavior of pulsating aurora, *J. Geophys. Res. Space Physics*, *122*, 5606–5618, doi:10.1002/2017JA024039.

Received 14 FEB 2017
Accepted 24 APR 2017
Accepted article online 26 APR 2017
Published online 11 MAY 2017

Occurrence and average behavior of pulsating aurora

N. Partamies[1,2], D. Whiter[3], A. Kadokura[4], K. Kauristie[5], H. Nesse Tyssøy[2,6], S. Massetti[7], P. Stauning[8], and T. Raita[9]

[1]Department of Arctic Geophysics, University Centre in Svalbard, Longyearbyen, Norway, [2]Birkeland Centre for Space Science, Bergen, Norway, [3]Department of Physics and Astronomy, University of Southampton, Southampton, UK, [4]Space and Upper Atmospheric Sciences Group, National Institute of Polar Research, Tokyo, Japan, [5]Arctic Research, Finnish Meteorological Institute, Helsinki, Finland, [6]Department of Physics and Technology, University of Bergen, Bergen, Norway, [7]INAF-IAPS, Institute for Space Astrophysics and Planetology, Rome, Italy, [8]Danish Meteorological Institute, Copenhagen, Denmark, [9]Sodankylä Geophysical Observatory, University of Oulu, Oulu, Finland

Abstract Motivated by recent event studies and modeling efforts on pulsating aurora, which conclude that the precipitation energy during these events is high enough to cause significant chemical changes in the mesosphere, this study looks for the bulk behavior of auroral pulsations. Based on about 400 pulsating aurora events, we outline the typical duration, geomagnetic conditions, and change in the peak emission height for the events. We show that the auroral peak emission height for both green and blue emission decreases by about 8 km at the start of the pulsating aurora interval. This brings the hardest 10% of the electrons down to about 90 km altitude. The median duration of pulsating aurora is about 1.4 h. This value is a conservative estimate since in many cases the end of event is limited by the end of auroral imaging for the night or the aurora drifting out of the camera field of view. The longest durations of auroral pulsations are observed during events which start within the substorm recovery phases. As a result, the geomagnetic indices are not able to describe pulsating aurora. Simultaneous Antarctic auroral images were found for 10 pulsating aurora events. In eight cases auroral pulsations were seen in the southern hemispheric data as well, suggesting an equatorial precipitation source and a frequent interhemispheric occurrence. The long lifetimes of pulsating aurora, their interhemispheric occurrence, and the relatively high-precipitation energies make this type of aurora an effective energy deposition process which is easy to identify from the ground-based image data.

1. Introduction

Pulsating aurora is often described as regions of weak emission turning on and off with a period of about 2–20 s [*Lessard*, 2012; *Yamamoto*, 1988]. The emission regions can be of different sizes, more regular arc-like structures or irregular patches. The range of pulsation periods can vary a lot even within the same event, and as pointed out by *Humberset et al.* [2016], the periodicity is rather irregular even for a single structure. Pulsating aurora is often observed embedded in substorm activity and is most prominent during substorm recovery phases and the morning sector aurora. The source for the particles causing the pulsating aurora has been attributed to wave-particle interaction due to chorus waves at the equatorial magnetosphere [*Lessard*, 2012, and references therein]. Chorus wave activity is triggered by cyclotron resonance instability with plasma sheet electrons that are injected into the inner magnetosphere during geomagnetic activity. Hence, the associated precipitation typically occurs at the equatorward part of the auroral oval [*Thorne et al.*, 2010].

A previous statistical study of pulsating aurora included 74 pulsating aurora events observed in the Time History of Events and Macroscale Interactions during Substorms (THEMIS) ground-based [*Donovan et al.*, 2006] auroral camera data in 2007–2008 [*Jones et al.*, 2011]. They found the most probable duration for the pulsating aurora to be 1.5 h with large variations. They further concluded that pulsating aurora events are common in general but most frequently occurring during the morning hours and hours after substorm breakups. Later on, *Jones et al.* [2013] reported on an extremely persistent pulsating aurora event over Canada and THEMIS which lasted for at least 15 h and covered at least 10 h of local time.

Not only are pulsating aurora events large in their spatial extent and long lasting in their lifetime, they are also often observed on both hemispheres simultaneously [*Watanabe et al.*, 2007, and references therein].

Single-pulsating aurora structures can appear both conjugate and nonconjugate in the interhemispheric observations. Similarly to the optical observations of pulsating aurora, signatures of chorus wave activity (a likely driver of the particle precipitation for pulsating aurora) have been observed on both hemispheres and over large local time spans simultaneously [e.g., *Manninen et al.*, 2012].

High-precipitation energies have been both modeled and observed during pulsating aurora. Observed electron density enhancements down to about 68 km suggest precipitation energies up to about 200 keV [*Miyoshi et al.*, 2015]. Lower band chorus waves were observed simultaneously by the Van Allen Probe A spacecraft. This wave activity was modeled to produce a wide range of precipitation energies into the ionosphere and was suggested to trigger both relativistic and auroral electrons. Precipitation energies over 10 keV during pulsating aurora have been further observed as a modulation of close range coherent echoes of the Super Dual Auroral Radar Network radars [*Milan et al.*, 2008]. The radar signatures showed a good correlation with cosmic radio noise absorption (CNA). The observed absorption values were low (at the level of 0.5 dB or even below) indicating that the fluxes of high-energy particles were also low.

A set of 21 pulsating aurora events were investigated by *Hosokawa and Ogawa* [2015]. They examined the evolution of the *E* region peak height and electron density from the European Incoherent Scatter (EISCAT) radar observations. The behavior of the ionization related to pulsating aurora was in good agreement with the optical characteristics of pulsating patches. The *E* region electron density peak height was found lower during the pulsating aurora as compared to the nonpulsating aurora observed during the same event. Furthermore, lower peak electron density heights were found to be associated with higher electron densities, and both lower peak heights and higher electron densities were observed toward the morning hours of magnetic local time. In addition, their results show an anticorrelation between the change in electron density peak heights and auroral electrojet (*AE*) index values during substorm activity prior to the pulsating aurora.

A more recent pulsating aurora study with EISCAT radar observations of electron densities showed electron density peak heights ranging between 93 and 100 km with the maximum at 96 km [*Oyama et al.*, 2016]. Auroral peak emission heights deduced by stereoscopic auroral imaging [*Kataoka et al.*, 2016] have resulted in even lower heights of 85–95 km during pulsating aurora, while simultaneously occurring discrete aurora gave peak emission heights of 100 km and above. These observations of low heights in peak emission and electron density have inspired investigations of chemical changes in the atmospheric composition due to the strong ionization. The chemical consequences of precipitating electrons with energies up to about 200 keV, as reported by *Miyoshi et al.* [2015], have been modeled by *Turunen et al.* [2016]. After 30 min of pulsating aurora type precipitation chemistry model calculations suggest a depletion in mesospheric odd oxygen of the order of several tens of percent. In the model results this was seen as significant increases in NO_x and HO_x species at and below the mesopause region. In particular, determining the NO_x production altitude is vital also to estimate its indirect effect due to transport on odd oxygen in the upper stratosphere [*Sinnhuber et al.*, 2014]. Hence, it is important to characterize and understand energetic electron precipitation to altitudes, where auroral electrons do not normally penetrate in substantial amounts.

While it is evident that the high-energy precipitation during pulsating aurora can be an important driver of mesospheric ozone depletion, little is known about how often and in which conditions this is the case. The aim of the current study is to examine properties for pulsating aurora in a statistical manner and throughout a solar cycle to outline the typical conditions and occurrences. As the first large statistical study, this lays the foundation for further development of proxies for high-energy precipitation based on ground-based auroral observations.

2. Ground-Based Auroral Camera Observations

In 1997–2007 the Magnetometers-Ionospheric Radars-All-sky Cameras Large Experiment (MIRACLE) network of all-sky cameras (ASC) [*Syrjäsuo et al.*, 1998; *Sangalli et al.*, 2011] included five identical instruments in the Fennoscandian Lapland with overlapping fields of view (FOV). Another similar camera pair has been in operation on Svalbard since 1999. The common imaging mode includes a green filtered image at 557.7 nm every 20 s, as well as blue (427.8 nm) and red (630.0 nm) line images once a minute. Usually, 1 s exposure time is used for the green emission and 2 s for the blue and red emission, although some short-term changes have been made over the course of the years. The typical imaging season in Lapland starts in September and ends in March. The images are automatically captured whenever the Sun is more than 10° below the horizon. This results in about 0.8 million images per year and per station. Pruning of these data separates images which

include aurora, making them easily available for further analysis. More details of the camera system, imaging, and the pruning procedure can be read in, e.g., *Partamies et al.* [2014].

In this study, we have used the keogram (quicklook) data to visually identify periods of pulsating aurora. Thumbnail images with 1 min time resolution have also been viewed to verify the detection of pulsating aurora and to fine-tune the beginning and end times of the intervals. This method is not exclusive by any means but provides an easy and relatively quick detection of large amount of samples. Individual pulsating structures with high pulsation frequencies cannot be detected, but our visual detection rather relies on identification of patchy auroral displays. We have further selected periods where the pulsating aurora structures cover large parts of the FOVs to facilitate further analysis of auroral peak emission heights. An automatic method introduced by *Whiter et al.* [2013] was applied for the whole pruned set of MIRACLE ASC images. The method is a modern version of triangulation assigning one height value for each image pair. An image pair means any two simultaneous images from neighboring ASC stations with overlapping FOVs. The brightness distributions from the two images are mapped both onto a set of horizontal planes and a grid of field lines. Peak emission height estimates are obtained for each mapping type separately, and when these agree, the height measurement is included in the statistical analysis. The method was validated with synthetic data and tested with real images for which the peak emission heights had previously been triangulated manually. The method is capable of resolving changes in peak emission heights of less than 1 km. The observed variations in the auroral emission heights are an order of magnitude larger [*Sangalli et al.*, 2011]. Since the pulsating aurora events for this study were selected to fill most of the FOV, the corresponding peak emission height value describes the average height of the pulsating structures. Many pulsating aurora intervals were observed to start during substorm activity. Substorm aurora is typically much more intense than pulsating aurora, and in case of a mixture of intense and faint aurora in the camera FOV, the height method typically assigns the height of the most intense emission to the whole image. We therefore require the pulsating aurora to be the most dominant feature in the image.

An example of pulsating aurora as seen in keogram data on 31 December 2003 is shown in Figure 1. Keograms from Kilpisjärvi (KIL, Glat 69.02°, CGMlat 65.94°), Kevo (KEV, Glat 69.76°, CGMlat 66.32°), Longyeabyen (LYR, Glat 78.20°, CGMlat 75.12°), and Ny-Ålesund (NAL, Glat 78.92°, CGMlat 75.25°) are organized so that south is to the bottom and north to the top of the figure. The distance between the Lapland and Svalbard camera stations is roughly 1000 km. The brightest stripes in the KIL and KEV keograms (the fourth and third panels) at about 18–20 and 22–24 UT on 30 December correspond to displays of substorm aurora. As the brightest emission after the latter substorm activity fades away, the diffuse emission starts to include thin stripes and larger faint patches at about 1 UT on 31 December. The whole auroral activity region moves north and out of the camera FOV at 03:30–04:00 UT. The thin stripes correspond to small pulsating patches turning on and off. The northward drift of the aurora is typical for morning hours when the Lapland region is turning away from the auroral oval. In the Svalbard keograms (Figures 1, first panel and 1, second panel) there are no obvious substorm signatures during the premidnight or midnight hours. However, faint diffuse aurora with thin stripes of pulsations can be seen first in the southern horizon at around 03:30 UT and later in the southern half of the FOVs until about 7 UT. In this example case the interval of the pulsating aurora for the current study is at 1–3 UT, but combining the Lapland and Svalbard data, the true pulsating aurora activity spans from midnight to about 7 UT. The keograms are constructed from images with 1 min cadence, which is a long time separation for single pulsating patches. Our identification method, however, benefits from the fact that many different pulsation frequencies take place simultaneously resulting in a patchy display of diffuse aurora.

This pulsating aurora event occurred during mild excursions of less than 70 nT in the local electrojet (*IL*) index. Figure 2 (top) shows the time evolution of *IL* index constructed from MIRACLE network magnetometer data to capture the magnetic disturbances in the time sector of optical and riometer observations. Larger variations are seen during substorm activity at about 19–20 UT and later around midnight, but during the observed pulsating aurora at about 1–3 UT, the magnetic deflections are minor. The cosmic radio noise absorption (CNA) measured by a wide beam (60°) La Jolla riometer (operated at 30.0 MHz) at Ivalo station, about 135 km south from KEV camera station, is displayed by the black curve in Figure 2 (bottom). The blue curve is CNA from Svalbard imaging riometer (IRIS, operated at 38 MHz) [*Stauning and Yamagishi*, 1995; *Stauning et al.*, 1995] calculated by averaging the absorption values from the four middle beams. During the pulsating aurora, absorption values from both riometers are well below 0.5 dB. A mild absorption peak in IRIS data of about 0.25 dB at 02:40–02:50 UT agrees with the diffuse aurora band expanding northward and appearing in the LYR and NAL keograms. When the pulsating aurora patches are closest to the zenith in the keograms at 4–6 UT, the

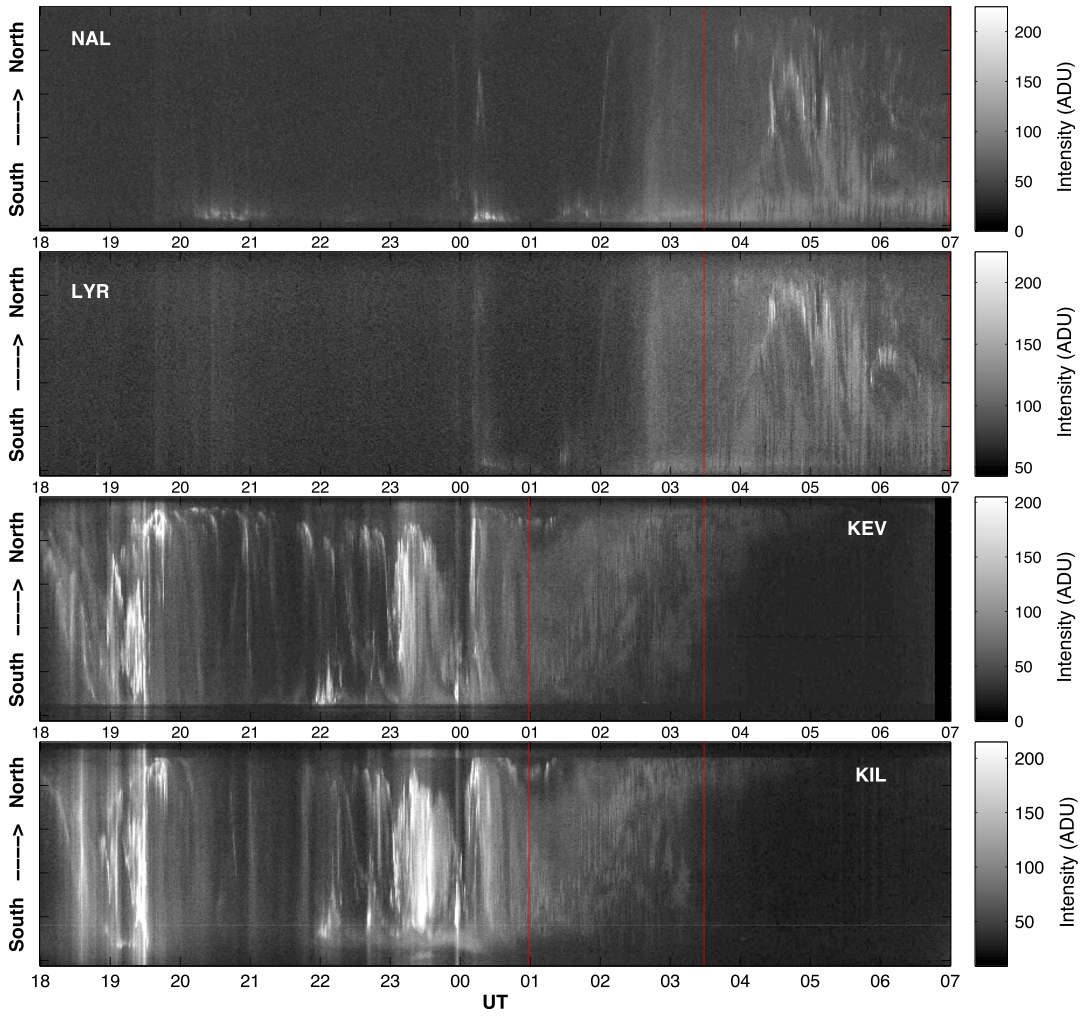

Figure 1. Keograms of (fourth panel) KIL and (third panel) KEV cameras in Lapland show substorm activity before UT midnight on 30 December 2003. Pulsating aurora starts to dominate the mainland station FOVs at around 1 UT, continues until about 3:30 UT, and slowly disappears northward. In the Svalbard keograms from (second panel) LYR and (first panel) NAL pulsating aurora appears at around 3:30 UT and is seen until about 7 UT in the morning. Periods when the pulsating aurora dominates the ASC FOVs are bracketed by vertical red lines. Zero epoch time for KIL and KEV, as used in our statistical study, is 1 UT. Magnetic midnight in Lapland is at about 21 UT.

absorption also fluctuates mildly (0.1–0.2 dB). The cadence of ASC data is not high enough for investigating the precise correspondence between absorption and optical intensity fluctuations. However, these observations suggest that the highest particle fluxes of soft precipitation (energies below 10 keV) which contribute to the enhanced conductivity and currents (*IL*) take place during the substorm activity prior to the pulsating aurora. The high-energy precipitation associated with the pulsating aurora comes in low flux values as indicated by low CNA levels.

ASC image inversion by *Janhunen* [2001] gives total electron energy flux distributions for auroral images. Four auroral images of different auroral features from KIL station were selected to examine how the energy flux changes over time. The method runs included upgrades on electron range and yield of blue photons according to *Sergienko and Ivanov* [1993], which were tested by *Partamies et al.* [2004]. Figure 3 displays images of diffuse nonpulsating aurora (00:25 UT) to pulsating arcs (01:10 UT), large elongated pulsating patches (02:12 UT), and small pulsating features (02:54 UT). An inverted energy flux of these four selected images (data not shown) decreases from about 10 to about 5, 3.5, and 2.5 mW/m^2, respectively. This energy flux decrease describes the change in the average auroral precipitation energies up to about 8 keV, which is the maximum energy in the inversion method. Low fluxes of higher energies are likely to remain more constant as the variations in absorption are not dramatic (within about 0.5 dB).

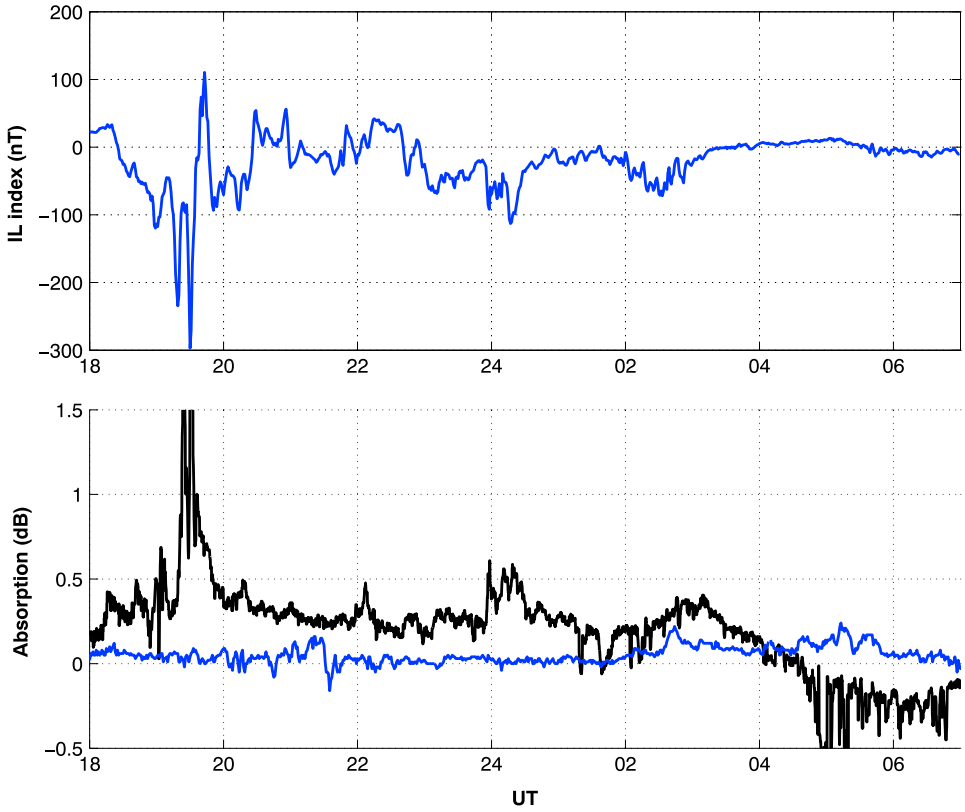

Figure 2. (top) Local electrojet (*IL*) index (nT) and (bottom) cosmic radio noise absorption from Ivalo (black) and Longyearbyen (blue) station for the sample event on 30–31 December 2003.

3. Occurrence of Auroral Pulsations and Their Relation to Magnetic Activity

The visual search described above resulted in detection of 398 periods of pulsating aurora in 1997–2007. The median duration of these events is 1.4 h and the total duration of the pulsating aurora sums up to 661 h, for when the auroral pulsations dominate the camera FOV. The majority of the pulsating aurora events lasted to the end of the imaging at dawn or until the pulsating patches drifted out of the FOV as the camera stations rotated away from the auroral oval. This suggests that rather than the pulsating aurora dying, it often moves out of the FOV or becomes undetectable by the increasing daylight. The duration values estimated based on the analyzed data set are thus underestimating the true lifetimes of auroral pulsations.

Typical magnetic activity during pulsating aurora is moderate at best. Planetary *Kp* index is 2–4, which is an average value for all auroral activity in the Lapland region [*Partamies et al.*, 2015]. The *AE* index typically experiences a mild increase (order of 100 nT) maximizing close to the start of the pulsating aurora event. The median

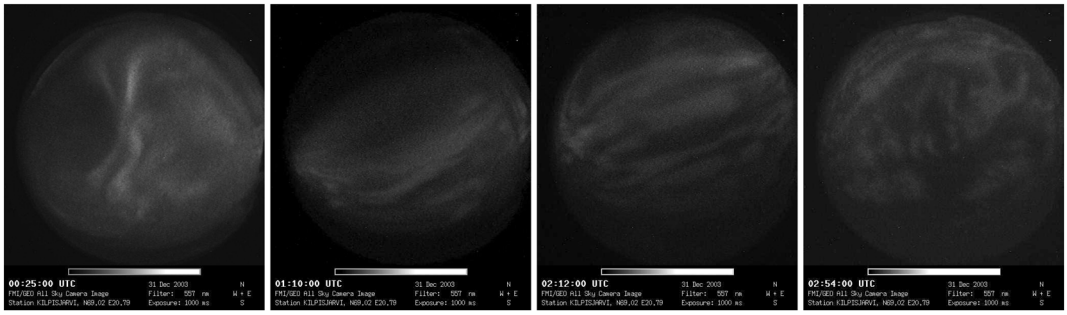

Figure 3. KIL auroral images of diffuse nonpulsating aurora (00:25 UT) to pulsating arcs (01:10 UT), large elongated pulsating patches (02:12 UT), and small pulsating features (02:54 UT). Image brightness has been enhanced for better visibility of the emission structures of interest.

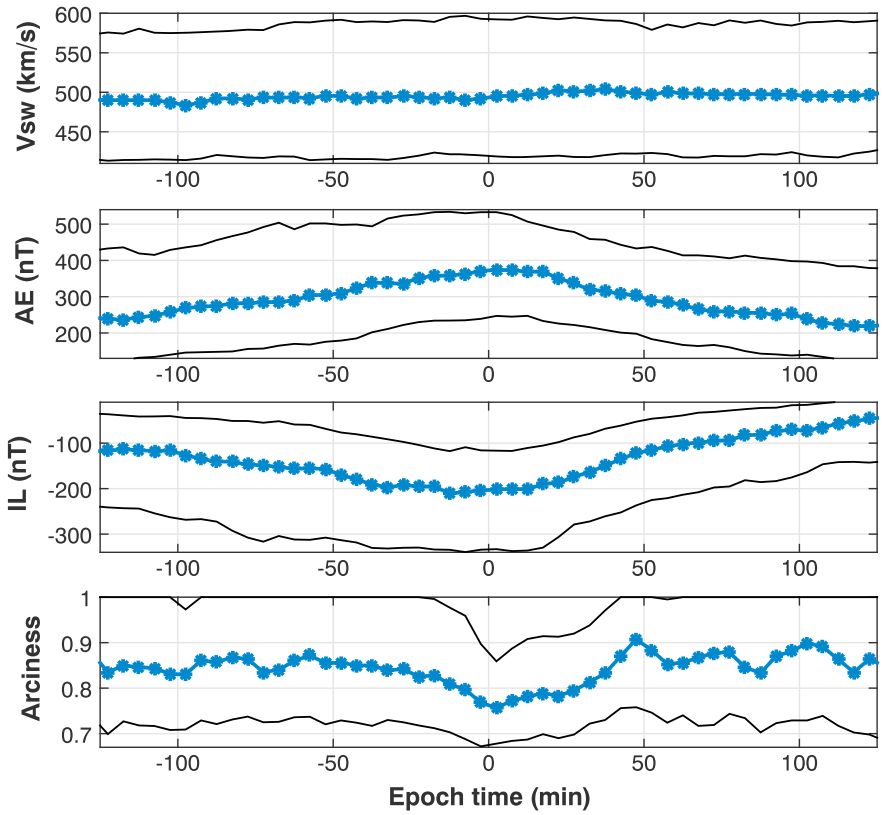

Figure 4. (first panel) Solar wind speed (km/s), (second panel) *AE* index (nT), (third panel) *IL* index (nT), and (fourth panel) arciness index as a function of epoch time in minutes. The blue curves are the median values and the black curves are 25th and 75th percentiles, respectively. Zero epoch time is the time when pulsating aurora becomes the dominant aurora type in a camera FOV. The ±2 h from the zero epoch time is shown because it captures the most dramatic changes.

index value stays under 500 nT (blue curve in Figure 4, second panel). Similarly, the typical local electrojet index (*IL*) value varies within the values of average substorm conditions (-200 nT$<IL<-100$ nT) but peaks at around the beginning of the pulsating aurora interval and typically recovers to the prepulsating event values at the beginning of the epoch (~ -100 nT) before the end of the pulsating aurora event (epoch time ~80 min). The decline in the magnetic indices during the pulsating aurora suggests that the pulsating aurora events mainly occur during the recovery of the magnetic activity. The median *Dst* index value for pulsating aurora is -28 nT. This is of the same order as that observed during average substorm events with auroral observations within the same region [*Partamies et al.*, 2015]. Pulsating aurora is thus clearly not related to geomagnetic storm activity, but rather to locally typical substorm activity which is already decaying at the time when the pulsating aurora takes over the auroral display.

Average solar wind speed of about 490 km/s is observed during the pulsating aurora periods (Figure 4, first panel) and the typical IMF magnitude is about 8 nT (data not shown). The range of variations (shown by the black percentiles) in the solar wind speed is large, but the behavior over the pulsating aurora events is steady. These values correspond to moderate to high driving. Furthermore, pulsating aurora were most common during the declining phase of the solar cycle in 2001–2003. The minimum occurrence rate based on our event list of the auroral pulsations is estimated to be about 10% of all aurora. This estimate is based on the number of images during the intervals of pulsating aurora in this study divided by the number of all images containing aurora (MIRACLE pruning, as described by *Partamies et al.* [2014]). For the same reasons our event durations are conservative, the occurrence rate estimate should also be considered a minimum. The annual occurrence of pulsating aurora mildly correlates with the annual averages of solar wind speed (Pearson correlation coefficient 0.6). This is in agreement with pulsating aurora being associated with high-energy precipitation and being most frequently observed during the declining phase of the solar cycle which is when the average solar wind speed is high [*Asikainen and Ruopsa*, 2016].

Table 1. Dates and Times of Interhemispheric Pulsating Aurora[a]

	Date	Time (NH)	Time (SH)
1	2000/9/22	00:00–02:30	00:00–01:12
2	2002/4/13	23:00–00:25	23:00–23:30
3	2003/3/15	01:20–03:05	00:00–00:20
4	2003/3/27	21:00–24:00	21:00–21:30
5	2003/4/3	23:59–01:12	23:55–01:30
6	2004/9/17	23:20–02:12	22:30–01:20
7	2005/3/8	20:30–21:30	21:00–21:10
8	2005/3/14	23:00–01:00	23:30–24:00

[a]Date format is year/month/day. Times are given in UT for Northern (NH) and Southern (SH) Hemispheres, respectively.

Auroral arciness [*Partamies et al.*, 2014] is an index describing the complexity of auroral structures. The calculation is based on the distribution of the emission brightness and its clustering in an image. Arciness value of unity corresponds to an arc or a multiple arc, while lower values of arciness relate to more complex structures. Similarly to peak emission heights, a single value of arciness is assigned for one image. Arciness averages to about 0.8 during pulsating aurora. The median epoch value (blue curve) in Figure 4 (fourth panel) shows steady values around 0.85 and a decrease down to about 0.75 by the start of the pulsating aurora. The decrease in arciness prior to the beginning of the pulsating aurora event may indicate that the temporal evolution from larger to smaller structures, as in the sample case in Figure 3, may be a typical behavior. The recovery of arciness back to the values around 0.85 takes place within 50 min after the start of the auroral pulsations. The structural changes in the aurora over the zero epoch time are not large, but more importantly, the auroral displays within the time frame of $\pm$2 h from the beginning of the pulsating aurora are not dominated by arc-like aurora (arciness equalling 1). Pulsating aurora rather emerges from complex structures and widespread emission.

Out of 10 events where simultaneous auroral images with clear skies were available from Syowa station in the Antarctic, eight events were observed to include pulsating aurora in the Southern Hemisphere as well. These events and their timings are given in Table 1. For northern hemispheric pulsating aurora the case 1 is observed at ABK, case 2 at MUO, and the rest at SOD station. Other pulsating events may appear during the same nights but the listed times are for the intervals with the closest correspondence between the two hemispheres. The Syowa station at −69.00°S and 39.58°E is equipped with an all-sky TV camera with high frame rate [e.g., *Sato et al.*, 2004]. The Syowa station has a conjugate location in Iceland which is about 2 h behind the Lapland local time. The strictly simultaneous imaging at Syowa and Lapland is only possible during about 2 months/yr. Therefore, the number of simultaneously captured clear and dark skies is rather small. The number of interhemispheric pulsating aurora within the sample, however, is very high. In three of the interhemispheric events (events 2, 4, and 5 in Table 1) the pulsating aurora starts at about the same time in both regions. An example of this type of events is shown by keograms in Figure 5 of 3 April 2003 at 19:00–01:30 UT. Irregular stripes of faint luminosity are seen in SOD (top) and Syowa (middle) station data after midnight. The high-resolution keogram of Syowa data (bottom) provides a more detailed view to the brightness variations. In another four events the time difference between the pulsating aurora observations is less than an hour (events 1 and 6–8 in Table 1), i.e., clearly less than the dislocation of the actual northern hemispheric conjugate region from Lapland would suggest. This indicates that the pulsating aurora often extends wider in azimuth than one station alone would be able to capture.

3.1. Pulsating Aurora Versus Substorm Phases

The majority of the pulsating aurora periods took place during substorm recovery phases (239 events or about 60% started in recovery) but some also during the expansion (124 events or about 31% started in expansion). The substorm phases are identified from the magnetic field measurements at the camera stations to provide the closest correspondence between the magnetic and optical auroral changes. Following our previous study, we use the local auroral electrojet index based on the camera station magnetograms (IL_{ASC}) and the substorm phases identified in this local index by *Partamies et al.* [2015]. The camera stations are located at the latitudes of average auroral activity in the MIRACLE network. Figure 6 shows the distribution of pulsating aurora within the substorm phases. The duration of each phase has been normalized to range from 0 to 1. The starts of the pulsating aurora intervals occur toward the end of expansion phases or during the early recovery phases. The pulsating aurora typically ends during a late substorm recovery phase or after the substorm activity. The substorm expansion and recovery phases, where pulsating aurora has been observed, have median durations of 0.5 and 1.4 h, respectively. This is approximately double compared to the median durations of all expansion and recovery phases detected in the region [*Partamies et al.*, 2015].

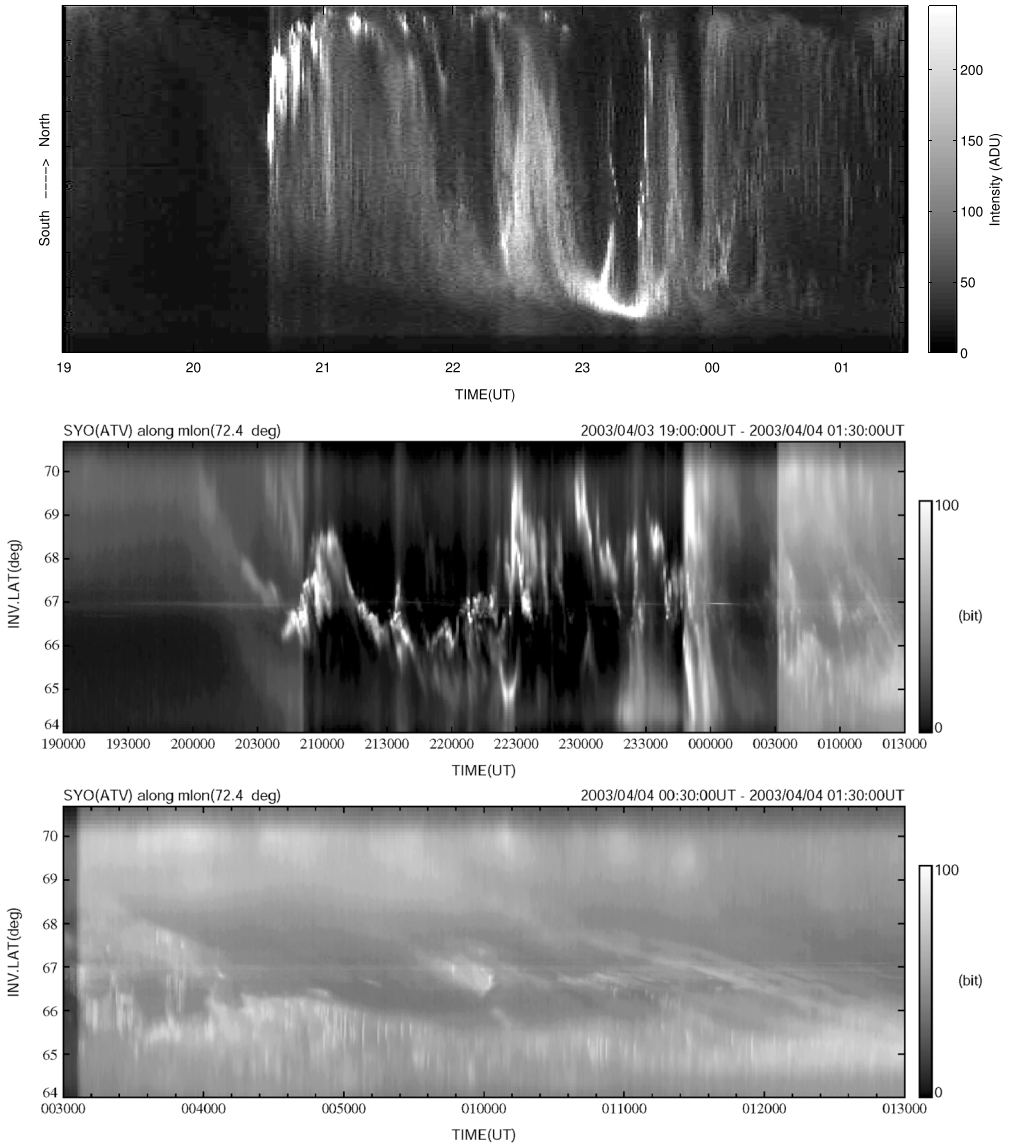

Figure 5. An example event of simultaneous interhemispheric pulsating aurora observed at (top) SOD, Finland and Syowa, (middle) Antarctica on 3 April 2003 at 19:00–01:30 UT. Pulsating aurora takes place over both stations after midnight and is seen as stripe-like features of faint emission. More detailed view of the irregular luminosity variations is shown by high-resolution (bottom) Syowa keogram of 00:30–01:30 UT. The brightness level change in Syowa data at 00:31 UT is due to an increased gain in the imaging system.

Half of the pulsating aurora events were identified in the data from SOD station (Glat 67.37°, CGMlat 63.92°) which is the most equatorward camera station of the five used in this study. This places most of the pulsating aurora to the equatorward part of the auroral oval. When pulsating aurora was observed to start within the substorm activity, it was always seen on the equatorward side of the more intense substorm aurora.

4. Peak Emission Heights During Pulsating Aurora

Auroral peak emission heights [*Whiter et al.*, 2013] have been analyzed for the pulsating aurora events. Figure 7 shows superposed epoch heights for ±2 h from the start of the pulsating aurora for green (left) and blue aurora (right). The median height values (blue curve) decrease by about 8 km at around the beginning of the events. This behavior is closely followed by the 10th and 90th percentiles (red curves). The height decrease is seen to start about 15–20 min prior to the zero epoch time. This is due to the fact that the first signs of pulsating aurora usually occur earlier than the start of the event on our event list, which is based on auroral

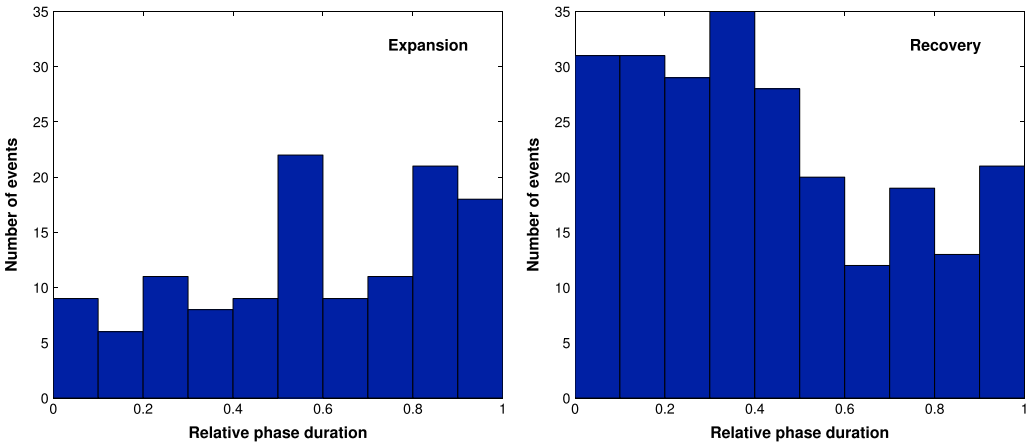

Figure 6. Occurrence distribution of pulsating aurora within substorm (left) expansion and (right) recovery phases. The duration of each substorm phase has been normalized to the scale 0–1. The number of events refers to the number of the pulsating aurora which start at that time of the substorm phase.

pulsations becoming the dominant feature in the auroral displays. Before the pulsating activity dominates the camera FOVs, we cannot be sure that the calculated height relates to the pulsating structures without examining every event separately. Thus, the observed height change relates to the change from other types of aurora to displays dominated by patchy pulsating aurora, whether it happens locally or due to the station rotating toward the morning sector auroral activity.

The median height curve nearly recovers within the median duration of 1.4 h (84 min). The 10th percentiles (lower red curves) show longer-lasting reduction in the peak emission height, suggesting that the highest precipitation energies require longer times to recover from the activity. The lowest auroral heights during pulsations reach down to about 90 km. Morning sector events (270 intervals) were related to larger height changes (about 10 km) and also lasted for twice as long on average as the midnight/evening sector events. The typical behavior of peak emission heights for blue and green emission is very similar. The blue emission height reduction just recovers faster, which may be affected by the smaller number of blue line images (hundreds of data points instead of thousands). Similar height changes have been observed in previous case studies of pulsating aurora [*Oyama et al.*, 2016]. While the actual median height values are not found significantly different during different storm or substorm phases, the evolution of the median height shows slower recovery during substorm recovery phases.

Peak emission heights during pulsating aurora as a function of UT is plotted in Figure 8. The blue symbols indicate average heights of each interval of auroral pulsations, while the red asterisks mark the hourly mean values of the average heights. The maximum occurrence of pulsating aurora is in the morning sector at

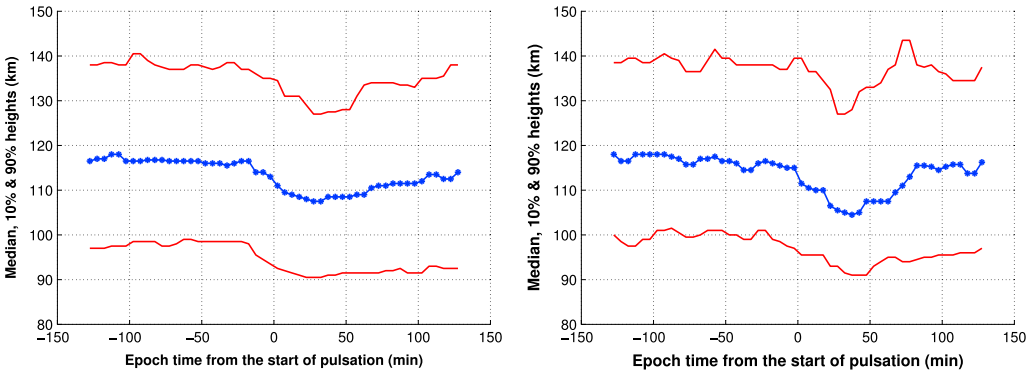

Figure 7. In the epoch time of minutes (*X* axis) (left) the median peak green emission height (blue curve) shows a decrease of about 8 km at the start of the pulsating aurora event (zero epoch). The 90th and 10th percentiles (red curves) illustrate that the lower the peak emission height the longer time it needs to recover. Each 5 min time slot includes 500–5000 data points (median of 2500).

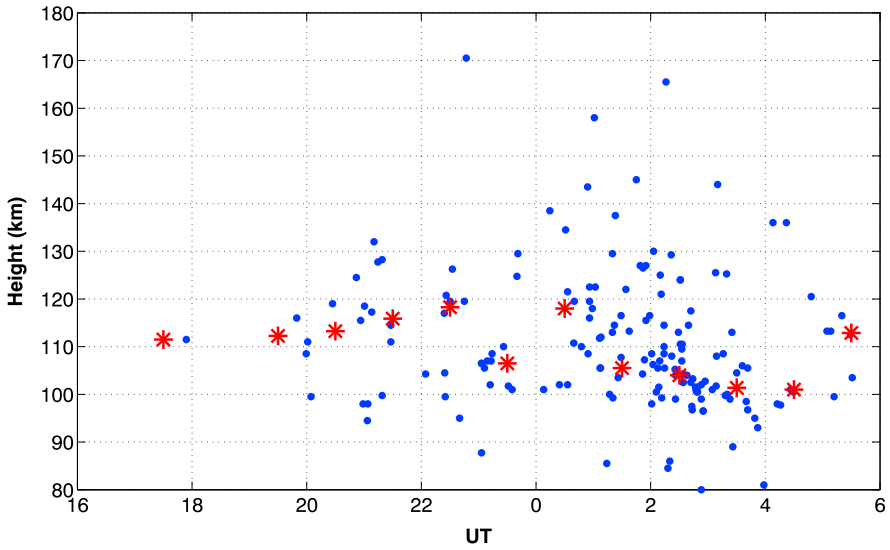

Figure 8. Auroral peak emission height evolution over the night is shown by median height values for each pulsating aurora interval (blue). Hourly averaged height values are plotted in red. Slight tendency for lower heights can be seen during the morning hours at 0–4 UT. Magnetic midnight in Lapland is at about 21 UT.

1–4 UT (~4–7 MLT). No pulsating-dominated auroral displays were found in the evening sector before 20 UT (~23 MLT). There is a mild tendency for lower heights after UT midnight, but that may be skewed by the increased number of events in that time sector. The scatter in the event-averaged heights (blue) also increases after midnight. In agreement with earlier observed changes in the *E* region peak electron density heights [*Hosokawa and Ogawa*, 2015], there are no significant changes in the heights prior to 6 MLT (3 UT in the MIRACLE sector). Past that time the number of optical observations becomes sparse.

Average peak emission heights were found to loosely relate to preceding geomagnetic activity. Periods of pulsating aurora were compared to the set of storm phases identified in the *Dst* index by a method similar to the substorm phase detection [*Partamies et al.*, 2013]. Storm recovery phases were defined to start from the *Dst* minimum value, which is required to be smaller than a long-term median value of −15 nT. Up to about 12 h from the start of the storm recovery phases, the pulsating aurora heights decrease in correlation (coefficient of about −0.7) with the time delay. The events starting within the first 2 h of storm recovery phases experience a large scatter in the emission heights, but the events starting later in the storm recovery phases decrease more coherently from 110 to 100 km.

5. Discussion

The typical occurrence of pulsating aurora determined from the current statistical study of about 400 events is in good agreement with previously reported case studies (references in *Lessard* [2012]) and smaller statistical approaches [e.g., *Jones et al.*, 2011]. In particular, the most common duration found here (1.4 h) closely agrees with that from a study by *Jones et al.* [2011] (1.5 h). The longest continuous pulsating aurora event in our database is about 7 h. However, our sample event (Figures 1–3) shows pulsating aurora being observed over Svalbard after being measured over the Lapland camera stations for about 2.5 h. Svalbard camera data are not included in the statistical analysis, but in the case of our sample event the high-latitude images about triples the event duration. Thus, durations in our data set should be considered as very conservative estimates knowing that many cases are not being observed until the end of pulsation in the aurora but rather until the end of good observing conditions. In fact, *Jones et al.* [2013] reported on an extremely persistent pulsating aurora event over Canada which lasted for at least 15 h, covering at least 10 h of local time. Our observations are combinations of lifetime of pulsating aurora and its local time extent due to the smaller common viewing area of the Lapland camera stations. Our observations are further given as lower limit estimates due to a limited common FOV of ground-based cameras and contamination of brighter auroral emission by softer precipitation. Another fact affecting the lifetime and occurrence estimates based on this data set is the sensitivity of the camera system. The analyzed data come from a camera system designed and built in the 1990s,

and pulsating aurora is generally reported to be low in intensity, so it is likely that some events with weakest emission intensity have not been detected. However, our list of pulsating aurora events is not meant to be exclusive but rather a statistically significant sample of events where the pulsating aurora dominates the ASC FOV. Another aurora type which may positively contribute to the patchiness of the all-sky view is flickering aurora [e.g., *Sandahl et al.*, 2011]. Flickering exhibits faster intensity fluctuations on smaller spatial extents as compared to pulsating aurora. It is partly beyond the ASC resolution in space and time, but for any still image during pulsating aurora, flickering aurora would cause similar patchy-looking display. With these facts in mind, the estimated minimum occurrence rate of about 10% is likely to be about double for the typical occurrence rate of pulsating aurora.

Ten pulsating aurora events over Lapland were accompanied by simultaneous good observing conditions at the Antarctic Syowa station. Eight out of 10 available events included simultaneous pulsating aurora on both hemispheres. Keeping in mind that good conditions for simultaneous optical observations on both hemispheres are rare, and only possible during a couple of months per year, the occurrence rate of 8/10 is high. Pulsating auroras have also previously been reported to occur on both hemispheres at the same time [*Watanabe et al.*, 2007]. This supports the idea of the source region for the precipitating particle being equatorial. The longitude difference between the Lapland and Syowa stations and the relatively short time difference between the observed pulsating aurora also suggest for larger azimuthal extent than what the camera FOVs can detect. However, studies by *Sato et al.* [2002, 2004] concluded that the particle source region for pulsating aurora may not be equatorial. In case of interhemispheric pulsating aurora but nonconjugate pulsating structures, the observed energy-time dispersion of the precipitating particles measured by FAST spacecraft indicated a particle source region off the equatorial plane, closer to the Earth. More detailed studies are required to resolve the accurate location of the particle source region along the field lines connecting the two hemispheres.

Pulsating aurora has mainly been associated with substorm recovery phases before [*Lessard*, 2012]. This is confirmed in the current study showing that the auroral pulsations start to dominate the auroral displays typically during the first half of the substorm recovery (for 60% of the cases). One has to remember, however, that our event selection criteria favors recovery phases over the expansion phases where brighter aurora plays a major role in the auroral displays. The fact that the substorm phases, within which the pulsating aurora were found, had lifetimes much longer than average substorm phases suggests that the magnetospheric substorm activity is an important preconditioning for the particle acceleration. The duration of the magnetic activity prior to the pulsating aurora occurrence may relate to the lifetime or efficiency of the acceleration process.

The observed peak emission height decrease of about 8 km at the start of the pulsating aurora-dominated interval is significant and systematic. The heights ranging down to about 90 km agree with the earlier pulsating aurora heights deduced in case studies by, e.g., *Kataoka et al.* [2016] and *Oyama et al.* [2016]. As concluded by *Hosokawa and Ogawa* [2015], the average electron density peak heights during pulsating aurora are about 10 km higher than the peak heights calculated during the pulsation On periods alone. This in mind, our height results, as averages, may be underestimates of the true height changes. This suggests an increase in precipitation energy as the auroral display transforms from substorm aurora to pulsating aurora. It is also likely that the more energetic precipitation already exists during the substorm breakup and expansion phase aurora, but it only shows up in the auroral height method when the bright aurora caused by high fluxes of softer precipitation decays. The durations of the pulsating aurora are longer than the typical durations of the expansion phases, so the longest-lasting part of the harder precipitation is being captured by the evolution of the peak emission heights. It is also interesting to note that the lower the peak emission heights (the higher the precipitation energies) the longer it takes for them to recover. This may further relate to the duration of earlier magnetic activity, as discussed above. The fact that the green and the blue emission heights undergo the same behavior suggests that the green emission, at least in case of pulsating aurora, comes primarily from an energy interchange process between atomic oxygen and molecular nitrogen. This would make the peak emission heights of the green auroral emission also carry information on the precipitation energy.

The decay of high fluxes of soft precipitation toward the substorm recovery phase and the time when pulsating aurora becomes a dominant aurora type explains why the peak emission height evolution does not correlate with magnetic indices. While the peak emission heights decrease reflects increased precipitation energies, the indices are more sensitive to high fluxes of softer particles which mainly contribute to the bright aurora and ionospheric currents.

Both the peak emission heights and the occurrence of pulsating aurora were found mildly correlated with the solar wind speed (correlation coefficients of 0.6–0.7). This agrees with the results by *Asikainen and Ruopsa* [2016] who concluded that the high-speed solar wind is the key term in driving high-energy precipitation. The level of solar wind driving during the pulsating aurora (wind speed of about 500 km/s) is comparable to the driving observed during sawtooth events and steady magnetospheric convections rather than isolated substorms as reported by, e.g., *Partamies et al.* [2009].

Structural changes in the pulsating aurora is an unresolved topic, largely because it is technically challenging to detect single pulsating patches [e.g., *Humberset et al.*, 2016] and to determine and track their sizes throughout the period of the pulsation. Based on the visual inspection of keograms in the search of pulsating aurora, our impression is that the patch size monotonically increases or decreases in most cases. The changes between arc-like and patch-like pulsating structures or the variation in the patch size may relate to precipitation energy changes. Our sample event shows a decay in the structure size and a decay in the total electron energy flux in the auroral energy range as a function of time after substorm. The decay of the pulsation structure size may well be a common feature after substorm activity, and the strength of the substorm activity prior to auroral pulsations may be a determining factor in the decay of the precipitation energy. As shown by the arciness evolution during the pulsating aurora, there is no clear trend in the arciness past the decrease at the beginning of the event and the recovery within 40–50 min. Thus, there may not be a systematic patch evolution but rather many different ways for the pulsating auroral structures to develop resulting in many different evolutions of brightness distributions which equal various different time series of arciness. A more dedicated method to resolve and follow the pulsating auroral structures as a function of a precipitation energy proxy is needed to answer the question of the importance of the patch size and its temporal changes.

6. Conclusions

As auroral intervals dominated by pulsating aurora are relatively easy to identify in auroral all-sky camera quicklook data, we performed a search of pulsating aurora periods in the MIRACLE all-sky camera data from five Lapland camera stations in 1996–2007. Comparison with camera data from the Antarctic Syowa station confirms that interhemispheric auroral pulsations are not uncommon, since eight out of 10 events with simultaneous data included pulsating auroral structures.

Key results from this study of about 400 pulsating aurora events include the typical conditions of moderate magnetic activity but rather high solar wind driving (speed of about 500 km/s and IMF about 8 nT). Auroral peak emission heights for green and blue line decrease systematically about 8 km at the beginning of the pulsating aurora event. This decrease suggests increase in precipitation energies and coincides with decaying magnetic activity. For the cases where the emission height decreased most, it also took longest to recover. Substorm recovery phases were found to trigger particularly long-lasting auroral pulsations which indicates that the magnetospheric substorm activity is needed to create favorable conditions for particle acceleration.

Acknowledgments
This work was partly supported by the Research Council of Norway under CoE contract 223252. Index data are from Kyoto World Data Center, solar wind data are from OMNIWeb. Ground magnetometer data used in this study are available at http://space.fmi.fi/image/. The authors thank S. Mäkinen, J. Mattanen, A. Ketola, and C.-F. Enell for careful maintenance of the MIRACLE camera network and data flow. MIRACLE ASC quicklook data are available at http://www.space.fmi.fi/MIRACLE/ASC/asc_keograms_00.shtml and at GAIA virtual observatory at http://gaia-vxo.org, while full resolution image data can be requested from FMI (kirsti.kauristie@fmi.fi). The Italian ASC in NAL is funded by PNRA. Sodankylä Geophysical Observatory riometer data quicklook plots can be browsed at http://www.sgo.fi/Data/Riometer/rioData.php and the data are available upon request. Imaging riometer data from Longyearbyen can be made available upon request.

References

Asikainen, T., and M. Ruopsa (2016), Solar wind drivers of energetic electron precipitation, *J. Geophys. Res. Space Physics*, *121*, 2209–2225, doi:10.1002/2015JA022215.

Donovan, E., et al. (2006), The THEMIS all-sky imaging array—System design and initial results from the prototype imager, *J. Atmos. Sol. Terr. Phys.*, *68*, 1472–1487, doi:10.1016/j.jastp.2005.03.027.

Hosokawa, K., and Y. Ogawa (2015), Ionospheric variation during pulsating aurora, *J. Geophys. Res. Space Physics*, *120*, 5943–5957, doi:10.1002/2015JA021401.

Humberset, B. K., J. W. Gjerloev, M. Samara, R. G. Michell, and I. R. Mann (2016), Temporal characteristics and energy deposition of pulsating auroral patches, *J. Geophys. Res. Space Physics*, *121*, 7087–7107, doi:10.1002/2016JA022921.

Janhunen, P. (2001), Reconstruction of electron precipitation characteristics from a set of multi-wavelength digital all-sky auroral images, *J. Geophys. Res.*, *106*, 18,505–18,516, doi:10.1029/2000JA000263.

Jones, S. L., M. R. Lessard, K. Rychert, E. Spanswick, and E. Donovan (2011), Large-scale aspects and temporal evolution of pulsating aurora, *J. Geophys. Res.*, *116*, A03214, doi:10.1029/2010JA015840.

Jones, S. L., M. R. Lessard, K. Rychert, E. Spanswick, E. Donovan, and A. N. Jaynes (2013), Persistent, widespread pulsating aurora: A case study, *J. Geophys. Res. Space Physics*, *118*, 2998–3006, doi:10.1002/jgra.50301.

Kataoka, R., Y. Fukuda, H. A. Uchida, H. Yamada, Y. Miyoshi, Y. Ebihara, H. Dahlgren, and D. Hampton (2016), High-speed stereoscopy of aurora, *Ann. Geophys.*, *34*, 41–44, doi:10.5194/angeo-34-41-2016.

Lessard, M. (2012), A review of pulsating aurora, in *Auroral Phenomenology and Magnetospheric Processes: Earth and Other Planets, Geophys. Monogr. Ser.*, vol. 197, edited by A. Keiling et al., pp. 55–68, AGU, Washington, D. C., doi:10.1029/2011GM001187.

Manninen, J., N. G. Kleimenova, O. V. Kozyreva, M. Parrot, T. Raita, and T. Turunen (2012), Experimental evidence of the simultaneous occurrence of VLF chorus on the ground in the global azimuthal scale—From pre-midnight to the late morning, *Ann. Geophys.*, *30*, 725–732, doi:10.5194/angeo-30-725-2012.

Milan, S. E., K. Hosokawa, M. Lester, N. Sato, H. Yamagishi, and F. Honary (2008), D region HF radar echoes associated with energetic particle precipitation and pulsating aurora, *Ann. Geophys.*, *26*, 1897–1904.

Miyoshi, Y., et al. (2015), Energetic electron precipitation associated with pulsating aurora: EISCAT and Van Allen Probe observations, *J. Geophys. Res. Space Physics*, *120*, 2754–2766, doi:10.1002/2014JA020690.

Oyama, S.-I., K. Shiokawa, Y. Miyoshi, K. Hosokawa, B. J. Watkins, J. Kurihara, T. T. Tsuda, and C. T. Fallen (2016), Lower thermospheric wind variations in auroral patches during the substorm recovery phase, *J. Geophys. Res. Space Physics*, *121*, 3564–3577, doi:10.1002/2015JA022129.

Partamies, N., P. Janhunen, K. Kauristie, S. Mäkinen, and T. Sergienko (2004), Testing an inversion method for estimating electron energy fluxes from all-sky camera images, *Ann. Geophys.*, *22*, 1961–1971, doi:10.5194/angeo-22-1961-2004.

Partamies, N., T. I. Pulkkinen, R. L. McPherron, K. McWilliams, C. R. Bryant, E. Tanskanen, H. J. Singer, G. D. Reeves, and M. F. Thomsen (2009), Different magnetospheric modes: Solar wind driving and coupling efficiency, *Ann. Geophys.*, *27*, 4281–4291, doi:10.5194/angeo-27-4281-2009.

Partamies, N., L. Juusola, E. Tanskanen, and K. Kauristie (2013), Statistical properties of substorms during different storm and solar cycle phases, *Ann. Geophys.*, *31*, 349–358, doi:10.5194/angeo-31-349-2013.

Partamies, N., D. Whiter, M. Syrjäsuo, and K. Kauristie (2014), Solar cycle and diurnal dependence of auroral structures, *J. Geophys. Res. Space Physics*, *119*, 8448–8461, doi:10.1002/2013JA019631.

Partamies, N., L. Juusola, D. Whiter, and K. Kauristie (2015), Substorm evolution of auroral structures, *J. Geophys. Res. Space Physics*, *120*, 5958–5972, doi:10.1002/2015JA021217.

Sandahl, I., U. Brändström, and T. Sergienko (2011), Fine structure of aurora, *Int. J. Remote Sens.*, *32*(11), 2947–2972, doi:10.1080/01431161.2010.541507.

Sangalli, L., N. Partamies, M. Syrjäsuo, C.-F. Enell, K. Kauristie, and S. Mäkinen (2011), Performance study of the new EMCCD-based all-sky cameras for auroral imaging, *Int. J. Remote Sens.*, *32*, 2987–3003, doi:10.1080/01431161.2010.541505.

Sato, N., D. M. Wright, Y. Ebihara, M. Sato, Y. Murata, H. Doi, T. Saemundsson, S. E. Milan, M. Lester, and C. W. Carlson (2002), Direct comparison of pulsating aurora observed simultaneously by the FAST satellite and from the ground at Syowa, *Geophys. Res. Lett.*, *29*(21), 2041, doi:10.1029/2002GL015615.

Sato, N., D. M. Wright, C. W. Carlson, Y. Ebihara, M. Sato, T. Saemundsson, S. E. Milan, and M. Lester (2004), Generation region of pulsating aurora obtained simultaneously by the FAST satellite and a Syowa-Iceland conjugate pair of observatories, *J. Geophys. Res.*, *109*, A10201, doi:10.1029/2004JA010419.

Sergienko, T. I., and V. E. Ivanov (1993), A new approach to calculate the excitation of atmospheric gases by auroral electron impact, *Ann. Geophys.*, *11*, 717–727.

Sinnhuber, M., B. Funke, T. von Clarmann, M. Lopez-Puertas, G. P. Stiller, and A. Seppälä (2014), Variability of NO_x in the polar middle atmosphere from October 2003 to March 2004: Vertical transport vs. local production by energetic particles, *Atmos. Chem. Phys.*, *14*, 7681–7692, doi:10.5194/acp-14-7681-2014.

Stauning, P., and H. Yamagishi, (1995), Imaging riometer installation Longyearbyen, *Tech. Rep.*, pp. 95–12, Danish Meteorol. Inst. (DMI), Svalbard.

Stauning, P., H. Yamagishi, M. Nishino, and T. J. Rosenberg (1995), Dynamics of cusp-latitude absorption events observed by imaging riometers, *J. Geomagn. Geoelectr.*, *47*, 823–845, doi:10.5636/jgg.47.823.

Syrjäsuo, M., et al. (1998), Observations of substorm electrodynamics using the MIRACLE network, in *Proceedings of the International Conference on Substorms-4, Lake Hamana, Japan, 9–13 Mar.*, edited by S. Kokubun and Y. Kamide, pp. 111–114, Terra Sci., Tokyo, Japan.

Thorne, R. M., B. Ni, X. Tao, R. B. Horne, and N. P. Meredith (2010), Scattering by chorus waves as the dominant cause of diffuse auroral precipitation, *Nature*, *467*, 943–946, doi:10.1038/nature09467.

Turunen, E., A. Kero, P. T. Verronen, Y. Miyoshi, S. Oyama, and S. Saito (2016), Mesospheric ozone destruction by high-energy electron precipitation associated with pulsating aurora, *J. Geophys. Res. Atmos.*, *121*, 11,852–11,861, doi:10.1002/2016JD025015.

Watanabe, M., A. Kadokura, N. Sato, and T. Saemundsson (2007), Absence of geomagnetic conjugacy in pulsating auroras, *Geophys. Res. Lett.*, *34*, L15107, doi:10.1029/2007GL030469.

Whiter, D. K., B. Gustavsson, N. Partamies, and L. Sangalli (2013), A new automatic method for estimating the peak auroral emission height from all-sky camera image, *Geosci. Instrum. Methods Data Syst.*, *2*, 131–144, doi:10.5194/gi-2-131-2013.

Yamamoto, T. (1988), On the temporal fluctuations of pulsating auroral luminosity, *J. Geophys. Res. Atmos.*, *93*, 897–911, doi:10.1029/JA093iA02p00897.